Vacuum–UV fluorescence spectroscopy of GeF4 in the 10–25 eV range

Baumgärtel, H; Jochims, H.w; Boyle, Kenneth; Seccombe, Dominic; Tuckett, Richard

DOI:
10.1016/S0009-2614(98)00881-1

ELSEVIER

25 September 1998

Chemical Physics Letters 294 (1998) 507–517

CHEMICAL PHYSICS LETTERS

Vacuum–UV fluorescence spectroscopy of GeF_4 in the 10–25 eV range

K.J. Boyle [a], D.P. Seccombe [a], R.P. Tuckett [a,*], H. Baumgärtel [b], H.W. Jochims [b]

[a] *School of Chemistry, University of Birmingham, Edgbaston, Birmingham B15 2TT, UK*

[b] *Institut fur Physikalische und Theoretische Chemie, Freie Universitat Berlin, Takustrasse 3, D-14195 Berlin, Germany*

Received 15 June 1998; in final form 27 July 1998

Abstract

Using synchrotron radiation in the 10–25 eV energy range, the vacuum–UV spectroscopy of GeF_4 using fluorescence excitation and dispersed emission techniques is reported. Rydberg states that photodissociate to a fluorescing fragment are assigned, and dispersed emission spectra are recorded at the peak energies of the excitation spectrum. Three channels are observed: $GeF_2\ \tilde{a}\,^3B_1$–$\tilde{X}\,^1A_1$ phosphorescence, $GeF_2\ \tilde{A}\,^1B_1$–$\tilde{X}\,^1A_1$ fluorescence, and emission from the $GeF_4^+\ \tilde{D}\,^2A_1$ state. Both $GeF_2\ \tilde{a}\,^3B_1$ and $\tilde{A}\,^1B_1$ probably form with F_2, and not 2F, as the other product. Using single-bunch mode, lifetimes of the $GeF_2\ \tilde{A}\,^1B_1$ and $GeF_4^+\ \tilde{D}\,^2A_1$ states are measured to be 9.3 ± 0.1 and 5.02 ± 0.01 ns, respectively.

1. Introduction

In two previous papers [1,2] we have reported the observation and analysis of the non-dispersed vacuum–UV (VUV) fluorescence and dispersed emission spectra following VUV excitation of CF_4 and SiF_4. Experiments were performed at the BESSY 1, Berlin synchrotron source, with excitation energies in the 10–25 eV range. These studies are of considerable applied interest due to the extensive use of plasma dry etching of masked silicon wafers by fluorine-containing gases (e.g. CF_4) to fabricate microelectronic devices (for example, see Ref. [3]). In this Letter we report the results of a complementary study on GeF_4, also of relevance to plasma etching. Unlike CF_4 and SiF_4 [4,5], the VUV absorption spectrum of GeF_4 has not been recorded below the LIF cutoff wavelength of 105 nm (i.e. $E > 12$ eV), and there has only been one report of a VUV absorption at 119 nm, corresponding to the $1t_1 \rightarrow \sigma^*$ electron excitation [6]. The electron energy loss spectrum (EELS) of GeF_4, a pseudo-absorption spectrum, has however been recorded with incident energies up to 200 eV at various scattering angles. Peaks in the 10–25 eV range have been assigned to excitations from the five outer-valence molecular orbitals [7].

In radio-frequency discharges of the kind used in plasma etching, fragment radicals and ions are created in an ill-defined manner by electrons whose energies span the 10–25 eV range. To understand the spectroscopy of the species formed in more detail, we use the more controllable method of photon excitation. Tunable VUV radiation from a synchrotron source is used to cover the same energy range as the plasma electrons. In the experiments

* Corresponding author. E-mail: r.p.tuckett@bham.ac.uk

0009-2614/98/$ - see front matter
PII: S0009-2614(98)00881-1

reported here, fluorescence from GeF_4 induced by tunable VUV radiation from the BESSY 1 synchrotron source is dispersed through a (secondary) UV/visible monochromator. Our experiments are sensitive to those Rydberg states of GeF_4 that photodissociate to an excited state of a fragment that fluoresces (process I), and to valence states of GeF_4^+ that fluoresce (process II):

$$GeF_4 + h\nu_1 \rightarrow GeF_4^*$$

$$\rightarrow GeF_3^* + F, \text{ or } GeF_2^* + 2F$$

$$\text{or } F_2GeF_3^* \text{ or } GeF_2^* \rightarrow GeF_3 \text{ or } GeF_2 + h\nu_2 \qquad \text{(I)}$$

and

$$GeF_4 + h\nu_1 \rightarrow (GeF_4)^* + e^-,$$

$$(GeF_4^+)^* \rightarrow GeF_4^+ + h\nu_2 . \qquad \text{(II)}$$

In CF_4 (SiF_4), emissions were observed in CF_3 (SiF_3), CF_2 (SiF_2) and CF_4^+ (SiF_4^+) [1,2]. In a complementary study on CCl_4, $SiCl_4$ and $GeCl_4$ [8], emissions from $GeCl_4$ were observed in $GeCl_2$, $GeCl_4^+$ and atomic Ge. Our results for GeF_4, in which emissions are observed from both the $\tilde{A}\,^1B_1$ and $\tilde{a}\,^3B_1$ excited states of GeF_2 and from GeF_4^+, complement an earlier study on GeF_4 performed at the Daresbury synchrotron source in the UK [9], where only photon energies greater than 20 eV were used and emission was detected by undispersed fluorescence. Using the single-bunch mode of BESSY 1, we have also measured the lifetimes of all the species produced in excited fluorescing states from both GeF_4 and SiF_4 photoexcited in the 10–25 eV range. The GeF_4 lifetimes confirm and extend those measured in our earlier study [9], the SiF_4 lifetimes also extend those measured very recently at BESSY 1 where an unexpected result for the $\tilde{a}\,^3B_1$ state of SiF_2 was obtained [2].

2. Experimental

Experiments were performed at the BESSY 1 synchrotron source in Berlin, using an apparatus described in detail elsewhere [2,10]. A 1.5 m normal-incidence monochromator (range, 7–35 eV; best resolution, 0.03 nm) attached to the 800 MeV electron storage ring provided the source of tunable VUV radiation. Fluorescence from the interaction of this beam with an effusive flow of gas (pressure, ca. 10^{-3} Torr) was dispersed by a 0.2 m focal length monochromator (Jobin Yvon H20UV). This secondary monochromator (recipricol dispersion 4 nm/mm) had no entrance slit and a fixed exit slit. The effective range of this secondary monochromator was 190–450 nm. In the spectroscopic experiments on GeF_4 using the multi-bunch, quasi-continuous mode of the synchrotron, fluorescence was detected by a photon-counting, red-enhanced Hamamatsu R6060 photomultiplier tube cooled to 280 K. Using the single-bunch mode of the synchrotron, the lifetime experiments on GeF_4 and SiF_4 used the same fast risetime (ca. 1.5 ns) Hamamatsu photomultiplier tube and a Jobin Yvon H20VIS monochromator (grating blaze, ca. 450 nm), which improved the sensitivity of this apparatus for $\lambda > 450$ nm. Using the multi-bunch mode, fluorescence excitation, action, and dispersed fluorescence spectra have been recorded. In the first two experiments, the VUV excitation energy was scanned, with detection of the fluorescence by the secondary monochromator set either to zero order or to a defined wavelength, λ_2. It was not possible to flux-normalise these spectra in situ to the incident VUV radiation, but the output from the grating in the primary VUV monochromator was known to vary by, at most, 30% over the 10–25 eV range. In the third experiment, the induced fluorescence was dispersed between 200 and 700 nm by the secondary monochromator for a fixed photoexcitation energy between 10 and 25 eV. No attempt has been made to allow for the changing sensitivity of the secondary monochromator detection system with wavelength. In the single-bunch mode, lifetimes of the emitters were measured by defining the VUV excitation energy (E_1) and the emission wavelength (λ_2), and measuring the decay of the fluorescence in real time using a time-to-amplitude converter and a multi-channel analyser. The range of lifetimes that can be measured accurately is limited to ca. 3–100 ns. Full details, and the method of analysis of the time-resolved decays using the programme FLUOR [11], are given elsewhere [2,10]. Germanium tetrafluoride gas (purity > 99%) was obtained from Fluorochem and used without further purification.

3. Thermochemistry of GeF_4 and GeF_4^+

The thermochemistry of the valence states of GeF_4^+ and the dissociation channels of GeF_4 to neutral products is shown in Table 1. The electron configuration of the five outer-valence molecular orbitals of GeF_4 is $\ldots(2a_1)^2(2t_2)^6(1e)^4(3t_2)^6(1t_1)^6$, where the numbering scheme excludes core orbitals. Photoelectron data are taken from two relatively old studies [12,13] but, to the best of our knowledge, they have not been improved upon. The energies of the neutral dissociation channels of GeF_4 are calculated from the 298 K heats of formation of GeF_x ($x = 1$–4) given by Harland et al. [14], with data for atomic Ge and F coming from Emsley [15]. These old data for GeF_x are only accurate to ± 0.1–0.3 eV, hence no attempt has been made to convert these dissociation energies to the more usually quoted values at 0 K. The energies of the $\tilde{a}\,^3B_1$ and $\tilde{A}\,^1B_1$ states of GeF_2 come from Martin and Merer [16,17] and Hauge et al. [18]. The excited state of $Ge(^3P_1)$ at 26.1 eV (Table 1) corresponds to that state of the Ge atom which is known to emit strongly to its ground state at 267 nm. This emission has been observed previously in a complementary study of $GeCl_4$ [8].

4. Results

The fluorescence excitation spectrum of GeF_4, recorded with the secondary monochromator set to zero order, between 10 and 25 eV is shown in Fig. 1a. The resolution of the VUV excitation source is 0.2 nm. The peaks observed at 13.3, 14.9 and 15.6 eV all have shapes characteristic of a resonant photoexcitation process. These energies lie below the adiabatic ionisation energy (IE) of GeF_4, and the peaks must therefore arise due to excitation of Rydberg states of GeF_4 which photodissociate to a fluorescing state of a neutral fragment (process I). By

Table 1
Energetics of dissociation channels of GeF_4 and GeF_4^+

Neutral/parent ion	Dissociation channel	Dissociation energy (eV)[a]	Adiabatic (vertical) IE (eV)[b]
	$Ge^*\ ^3P_1\ (4p^15s^1) + 4F$	26.1	
	$Ge\ ^3P_0\ (4p^2) + 4F$	21.4	
$GeF_4^+\ \tilde{D}\,^2A_1$			21.1[c] (21.3)
$\tilde{C}\,^2T_2$			18.2[d] (18.5)
$\tilde{B}\,^2E$			(17.0)
$\tilde{A}\,^2T_2$			(16.5)
$\tilde{X}\,^2T_1$			15.7[d] (16.1)
	$GeF\ X\,^2\Pi + 3F$	16.4	
	$GeF\ X\,^2\Pi + F_2 + F$	14.8	
	$GeF_2\ \tilde{A}\,^1B_1 + 2F$	15.4[e]	
	$GeF_2\ \tilde{A}\,^1B_1 + F_2$	13.8	
	$GeF_2\ \tilde{a}\,^3B_1 + 2F$	13.8[f]	
	$GeF_2\ \tilde{a}\,^3B_1 + F_2$	12.2	
	$GeF_2\ \tilde{X}\,^1A_1 + 2F$	10.0	
	$GeF_2\ \tilde{X}\,^1A_1 + F_2$	8.4	
	$GeF_3\ \tilde{X}\,^2A_1\ (?)^g + F$	5.4	
$GeF_4\ \tilde{X}\,^1A_1$			0

[a] Thermochemistry from Harland et al. [14].
[b] Photoelectron data from Cradock [13] unless otherwise stated.
[c] This work.
[d] Bassett and Lloyd [12].
[e] Hauge et al. [18].
[f] Martin and Merer [16].
[g] Symmetry of the ground electronic state of the CF_3 radical assuming C_{3v} symmetry [19].

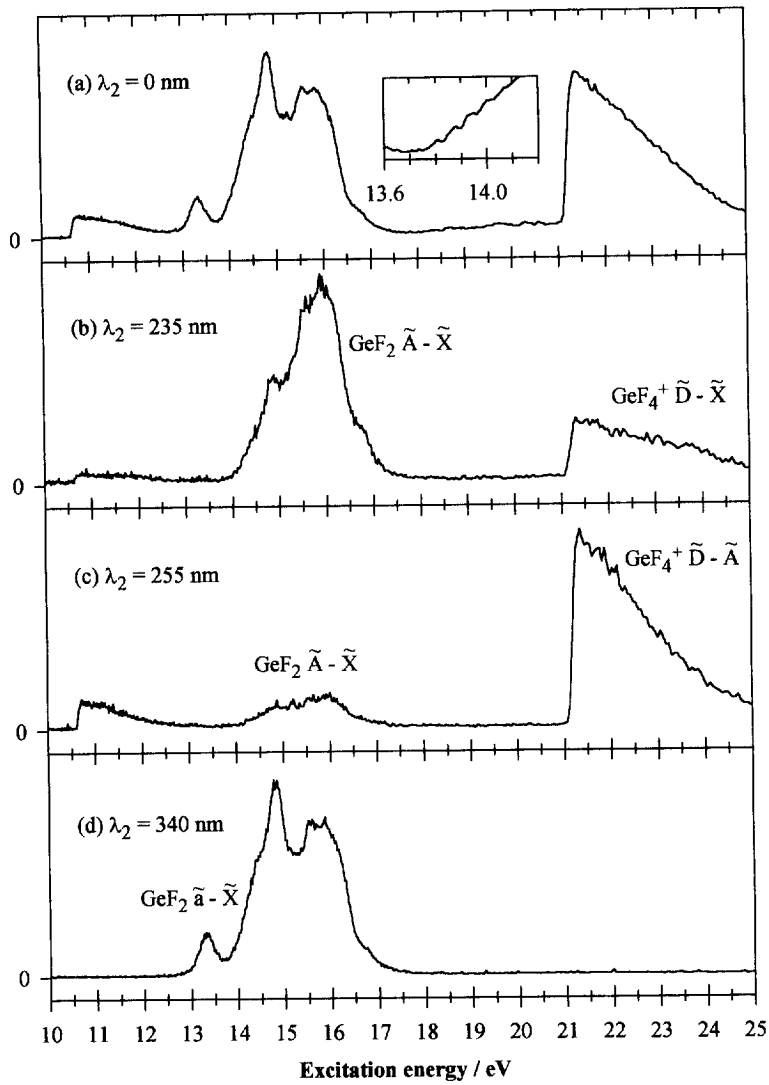

Fig. 1. Fluorescence excitation spectra of GeF_4 between 10 and 25 eV recorded at an optical resolution of 0.2 nm. Fluorescence has not been normalised to the VUV radiation from the primary monochromator. In (a) undispersed fluorescence ($\lambda_2 = 0$) was detected. In (b–d), action spectra were recorded for detection of fluorescence at (b) 235 ± 4 nm, (c) 255 ± 4 nm, and (d) 340 ± 4 nm. These three wavelengths correspond primarily to the peaks of the GeF_2 $\tilde{A}\,^1B_1$–$\tilde{X}\,^1A_1$, GeF_4^+ $\tilde{D}\,^2A_1$–$\tilde{A}\,^2T_2$ and GeF_2 $\tilde{a}\,^3B_1$–$\tilde{X}\,^1A_1$ emissions, respectively. Note that (b) and (c) contain minor contributions from GeF_4^+ $\tilde{D}\,^2A_1$–$\tilde{X}\,^2T_1$ and GeF_2 $\tilde{A}\,^1B_1$–$\tilde{X}\,^1A_1$ emissions, respectively.

contrast, the peak observed with a threshold of 21.1 eV and a maximum at 21.3 eV has a shape characteristic of a non-resonant photoionisation process (process II), in that the fluorescence signal remains non-zero for energies well in excess of threshold because the ejected photoelectron carries off the excess energy. These latter energies correspond to the adiabatic and vertical IEs of the $(2a_1)^{-1}$ fourth excited state of GeF_4^+ with $\tilde{D}\,^2A_1$ symmetry. Emission from this state has been observed before using electron beam [20], VUV photon [9] and fast H^+ beam [21] excitation of GeF_4, and the corresponding state of both CF_4^+ and SiF_4^+ exhibits radiative decay [22,23]. The weak non-resonant peak with threshold at 10.55 eV arises due to second-order radiation at 21.1 eV from the primary monochromator.

Dispersed spectra (Fig. 2) were recorded at the energies of the four major peaks in the fluorescence excitation spectrum. For excitation energies below the IE of GeF_4 (Fig. 2a–c), the spectrum is dominated by a broad band, peaking at 340 nm and spanning 300–380 nm, which is assigned to the spin-forbidden $\tilde{a}\,^3B_1$–$\tilde{X}\,^1A_1$ transition in GeF_2 [16,17]. For energies above 14 eV, a weaker band, peaking at 235 nm and spanning 215–265 nm, is observed which is assigned to the spin-allowed $\tilde{A}\,^1B_1$–$\tilde{X}\,^1A_1$ transition also in GeF_2 [18]. For an excitation energy of 21.4 eV (Fig. 2d) corresponding to emission from the $\tilde{D}\,^2A_1$ state of GeF_4^+, bands are observed at 230, 255, 288 and 400 nm. They correspond to the $\tilde{D}\,^2A_1$–$\tilde{X}\,^2T_1$, $\tilde{D}\,^2A_1$–$\tilde{A}\,^2T_2$, $\tilde{D}\,^2A_1$–$\tilde{B}\,^2E$ and $\tilde{D}\,^2A_1$–$\tilde{C}\,^2T_2$ transitions in GeF_4^+, respectively. The $\tilde{D}$–$\tilde{X}$ and $\tilde{D}$–$\tilde{B}$ transitions are orbitally forbidden if the lower states retain tetrahedral symmetry,

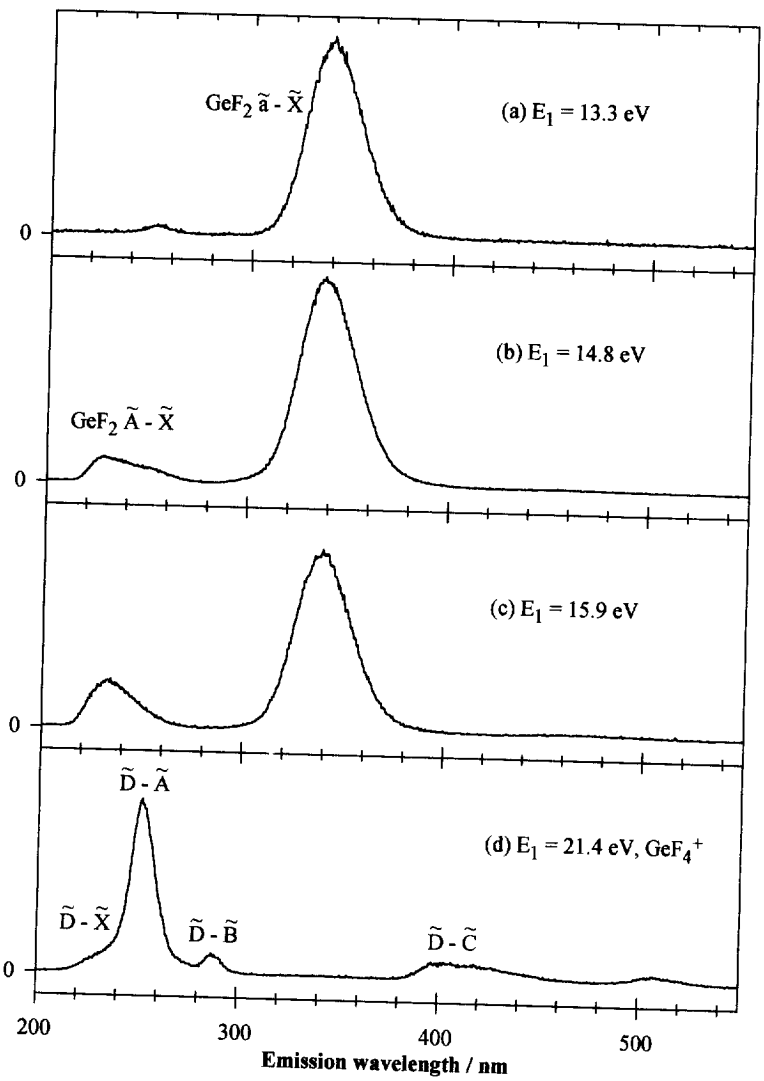

Fig. 2. Dispersed emission spectra for GeF_4 photoexcited at (a) 13.3, (b) 14.8, (c) 15.9 and (d) 21.4 eV. The optical resolution was 4 nm. No attempt has been made to allow for the variation of sensitivity of the detection system with wavelength, but it is predicted to decrease rapidly for $\lambda > 450$ nm.

but this selection rule is relaxed if either the $\tilde{X}\,^2T_1$ or $\tilde{B}\,^2E$ non-singly-degenerate states distort by the Jahn–Teller effect.

Action spectra were recorded at λ_2 values of 235, 255 and 340 nm, corresponding primarily to the GeF_2 $\tilde{A}$–$\tilde{X}$, GeF_4^+ $\tilde{D}$–$\tilde{A}$ and GeF_2 $\tilde{a}$–$\tilde{X}$ emissions, respectively (Fig. 1b–d). However, the action spectrum at 235 nm has minor contributions from GeF_4^+ $\tilde{D}$–$\tilde{X}$, that at 255 nm from GeF_2 $\tilde{A}$–$\tilde{X}$ emissions. These spectra were recorded after the dispersed spectra had been recorded, but they are displayed with the fluorescence excitation spectrum in Fig. 1 because in all cases it is the VUV excitation energy that is scanned. The 255 nm action spectrum, as expected, is dominated by a sharp threshold at 21.1 eV, the adiabatic IE of the $(2a_1)^{-1}$ state of GeF_4^+. The 340 nm action spectrum is very similar to the fluorescence excitation spectrum (Fig. 1a) over the 13–17 eV range, implying that a major photodissociation pathway of these Rydberg states of GeF_4 between these energies is to populate the $\tilde{a}\,^3B_1$ state of GeF_2. The 235 nm action spectrum suggests that as the photon energy increases over this range, there is an increased branching ratio to the $\tilde{A}\,^1B_1$ state of GeF_2. Note that these spectra do not reveal absolute values of the branching ratio to either the $\tilde{a}\,^3B_1$ or the $\tilde{A}\,^1B_1$ states of GeF_2 at any photon energy, nor do they reveal the importance of these channels compared to photodissociation to the ground state of GeF_2. The experimental thresholds for production of GeF_2 $\tilde{a}\,^3B_1$ and $\tilde{A}\,^1B_1$ are determined to be 12.8 ± 0.2 and 14.0 ± 0.2 eV, respectively.

Lifetimes of the $\tilde{a}\,^3B_1$ and $\tilde{A}\,^1B_1$ states of GeF_2 and the $\tilde{D}\,^2A_1$ state of GeF_4^+ were measured with E_1 and λ_2 values set accordingly (top half of Table 2). The lifetime of the $\tilde{a}\,^3B_1$ state of GeF_2 was too long to measure with the timing profile of the BESSY 1 synchrotron (orbit time, 208 ns), such that the decay was absolutely flat over the multi-channel analyser (Fig. 3c) with the time-to-amplitude converter set to a full range of 200 ns. We conclude that the lifetime of this state is greater than ca. 500 ns. Lifetimes of the $\tilde{A}\,^1B_1$ state of GeF_2 and the $\tilde{D}\,^2A_1$ state of GeF_4^+ (decays shown in Fig. 3b,a) were measured to be 9.3 ± 0.1 and 5.02 ± 0.01 ns, respectively. During these experiments, we also remeasured the lifetimes

Table 2
Lifetimes of emission bands observed from VUV excitation of GeF_4 (top half) and SiF_4 (bottom half) in the 10–25 eV range

E_1 (eV)	λ_2 (nm)[a]	τ (ns)	Reduced χ^2	Emitter
14.8	340	flat decay[b]		GeF_2 $\tilde{a}\,^3B_1$
15.9	235	9.3 ± 0.1	2.67	GeF_2 $\tilde{A}\,^1B_1$
21.4	255	5.02 ± 0.01	1.07	GeF_4^+ $\tilde{D}\,^2A_1$[c]
21.4	288	5.15 ± 0.03	1.17	GeF_4^+ $\tilde{D}\,^2A_1$[d]
21.4	400	5.05 ± 0.04	0.90	GeF_4^+ $\tilde{D}\,^2A_1$[e]
13.0	480	5.5 ± 0.2	1.11	SiF_3^*
15.9	400	3.3 ± 0.4	1.50	SiF_2 $\tilde{a}\,^3B_1$[f]
18.1	232	9–12[g]	1.2–1.5[g]	SiF_2 $\tilde{A}\,^1B_1$
21.8	304	9.13 ± 0.03	1.28	SiF_4^+ $\tilde{A}\,^2A_1$[h]

[a]The exit slit of the secondary monochromator was 2 mm (i.e. a wavelength resolution of 8 nm) for all the GeF_4 measurements and the SiF_4 measurement at 21.8 eV. For the other SiF_4 measurements, the wavelength resolution was degraded to ± 50 nm.
[b]With the signal-to-noise ratio of this spectrum (Fig. 3c), we assume that a flat decay implies $\tau >$ ca. 500 ns.
[c]Emission monitored via the GeF_4^+ $\tilde{D}\,^2A_1$–$\tilde{A}\,^2T_2$ transition centred at 255 nm.
[d]Emission monitored via the GeF_4^+ $\tilde{D}\,^2A_1$–$\tilde{B}\,^2E$ transition centred at 288 nm.
[e]Emission monitored via the GeF_4^+ $\tilde{D}\,^2A_1$–$\tilde{C}\,^2T_2$ transition centred at 400 nm.
[f]Almost certainly, this value is the inter-system crossing lifetime of vibrational levels of SiF_2 $\tilde{a}\,^3B_1$ to high vibrational levels of the electronic ground state, not the radiative lifetime of the $\tilde{a}\,^3B_1$ state.
[g]Unstable fit; the value of the lifetime depends upon the initial parameters given to the fit, and the channels over which the decay is fit. In our earlier measurement, we obtained 11.2 ± 1.5 ns [2].
[h]Emission monitored via the SiF_4^+ $\tilde{D}\,^2A_1$–$\tilde{A}\,^2T_2$ transition centred at 304 nm.

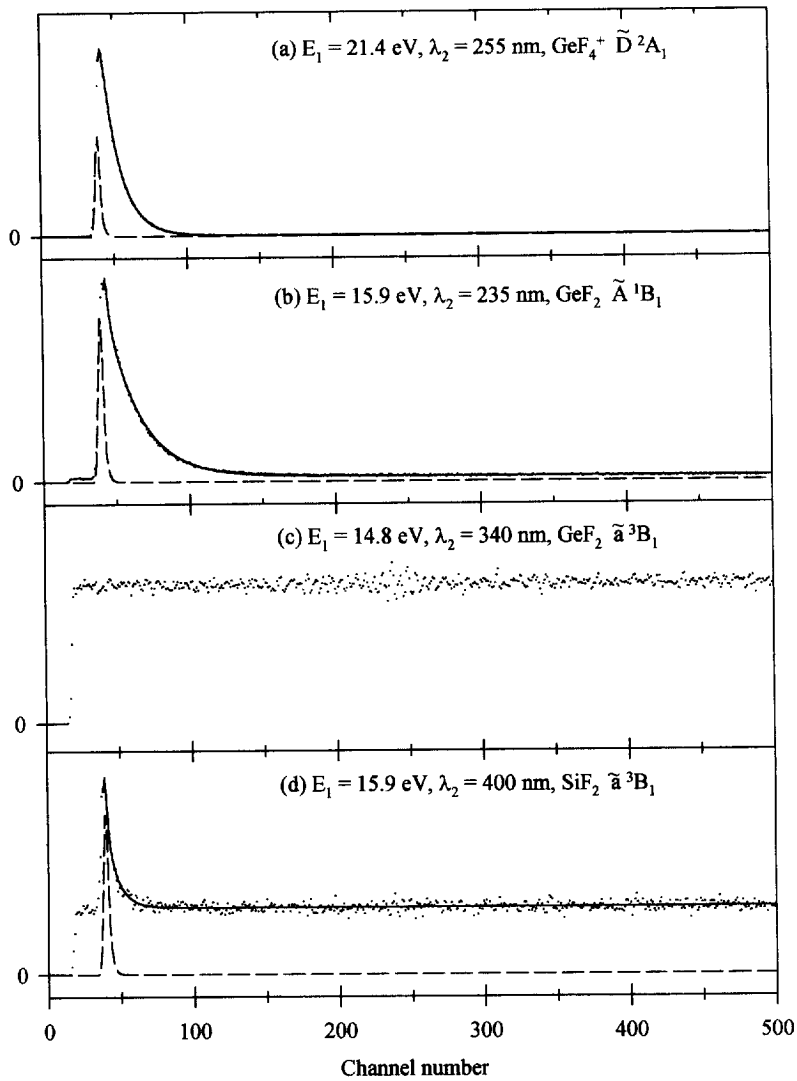

Fig. 3. Decay of the fluorescence following excitation of GeF_4 at (a) 21.4, (b) 15.9 and (c) 14.8 eV with single-bunch, pulsed radiation from the BESSY 1 synchrotron source. The secondary monochromator is set to a λ_2 value shown in the figure, and the emitting state is also shown. Each spectrum shows the experimental points, the prompt signal (dashed line), and the fit to the data (solid line) using the method described elsewhere [2,10,11]. The time calibration is 0.4137 ns per channel. In (a) and (b) the lifetimes are 5.02 ± 0.01 and 9.3 ± 0.1 ns, respectively. In (c) the decay of the signal is essentially flat, and we conclude the lifetime of the $\tilde{a}\,^3B_1$ state of GeF_2 is greater than ca. 500 ns. In (d), the decay of the fluorescence from the $\tilde{a}\,^3B_1$ state of SiF_2 is shown. By comparison with (c), there is now a fast decay component with a lifetime of 3.3 ± 0.4 ns.

of the same states of SiF_2 and SiF_4^+ (bottom half of Table 2), since a very surprising result for the $\tilde{a}\,^3B_1$ state of SiF_2 was obtained when the initial measurements were made [2]. The very short lifetime of the $\tilde{a}\,^3B_1$ state of SiF_2 (3.3 ± 0.4 ns, Fig. 3d) is confirmed (see Section 5). It is noted that there is no evidence for emission in the GeF_3 free radical. In particular, there is no analogous band to the very

broad band in the visible region observed in the SiF_3 radical [24] whose lifetime we measured to be 3.9 ns in our earlier measurements [2].

5. Discussion

First, we discuss the assignment of the Rydberg peaks of GeF_4 between 13 and 17 eV. The assignment of a Rydberg transition, energy E, relies upon the IE of the state of the parent ion to which the Rydberg state converges through the well-known formula

$$E = \mathrm{IE} - \frac{R_H}{(n-\delta)^2} \quad (3)$$

where R_H is the Rydberg constant and δ is the quantum defect of the Rydberg orbital of principal quantum number n to which the electron has been promoted. We use the vertical, and not the adiabatic, IE in such calculations. The main reason for this is that resolved vibrational structure is rarely resolved in any of the Rydberg transitions, so each band represents a convolution of many vibrational components, each with its own Franck–Condon factor. Assuming that there is no change in geometry between a Rydberg state and the state of the parent ion to which it converges and that autoionisation effects are small, the peak of an unresolved photoelectron band (i.e. the vertical IE)) also corresponds to the maximum in the Franck–Condon-weighted vibrational envelope. Under these circumstances, it seems appropriate to assign peak positions in the Rydberg spectra by convergence on the vertical IE of the parent ion. Approximate quantum defects for ns, np and nd Rydberg orbitals centred on a Ge (F) atom are predicted to be $\delta = 2.8$ (1.2), 2.3 (0.7_5) and 1.0 (0.0), respectively [25]. Using vertical IEs for the $(1t_1)^{-1}$, $(3t_2)^{-1}$ and $(1e)^{-1}$ molecular orbitals of GeF_4 of 16.1, 16.5 and 17.0 eV [13], respectively,

Table 3
Peak positions and assignments from fluorescence excitation spectroscopy of the Rydberg and ionic states of GeF_4 in the 12–25 eV range that lead to fluorescence, and assignments of the fluorescing fragments/ions and their lifetimes

E (eV)[a]	Assignment	IE − E (eV)	$n-\delta$	δ[b]	Emitter	Lifetime (ns)
13.3	$(1t_1)^{-1}3p$	2.8	2.20	0.80	GeF_2 $\tilde{a}\,^3B_1$	> ca. 500
	or $(1e)^{-1}3s$[c]	3.7	1.92	1.08		
14.0[d]	$(3t_2)^{-1}3p$	2.5	2.33	0.67	GeF_2 $\tilde{a}\,^3B_1$	> ca. 500
14.6[e]	$(1e)^{-1}3p$	2.4	2.38	0.62	GeF_2 $\tilde{a}\,^3B_1$	> ca. 500
					GeF_2 $\tilde{A}\,^1B_1$	9.3 ± 0.1
14.9	$(1t_1)^{-1}4p$	1.2	3.36	0.64	GeF_2 $\tilde{a}\,^3B_1$	> ca. 500
	or $(3t_2)^{-1}4s$	1.6	2.91	1.09	GeF_2 $\tilde{A}\,^1B_1$	9.3 ± 0.1
	or $(2t_2)^{-1}3s$	3.6	1.94	1.06		
15.6	$(3t_2)^{-1}5s$	0.9	3.89	1.11	GeF_2 $\tilde{a}\,^3B_1$	> ca. 500
	or $(3t_2)^{-1}4d$	0.9	3.89	0.11	GeF_2 $A\,^1B_1$	9.3 ± 0.1
	or $(1e)^{-1}4p$	1.4	3.12	0.88		
15.9	$(3t_2)^{-1}6s$	0.6	4.76	1.24	GeF_2 $\tilde{a}\,^3B_1$	> ca. 500
	or $(2t_2)^{-1}3p$	2.6	2.29	0.71	GeF_2 $\tilde{A}\,^1B_1$	9.3 ± 0.1
16.7[e]	$(2t_2)^{-1}4s$	1.8	2.75	1.25	GeF_2 $\tilde{a}\,^3B_1$	> ca. 500
					GeF_2 $\tilde{A}\,^1B_1$	9.3 ± 0.1
21.1[f]	$(2a_1)^{-1} \rightarrow GeF_4^+(\tilde{D}\,^2A_1) + e^-$				GeF_4^+ $\tilde{D}\,^2A_1$	5.02 ± 0.01

[a] Effects of second-order radiation producing GeF_4^+ $\tilde{D}$-state emission at excitation energies less than 21.2 eV are ignored in this table.
[b] Quantum defect, δ, defined by the equation $E = \mathrm{IE} - [R_H/(n-\delta)^2]$, where R_H is the Rydberg constant and n is the principal quantum number of the Rydberg orbital. Calculated using the appropriate vertical ionisation potentials for GeF_4 from HeI photoelectron spectroscopy [13].
[c] Optically forbidden transition.
[d] Vibrational structure in the band with spacing of ca. 0.06 ± 0.01 eV or 480 ± 80 cm^{-1}.
[e] Shoulder.
[f] Threshold for fluorescence, not peak position.

we can assign the transitions to the Rydberg states of GeF_4 between 13 and 17 eV (Table 3). The derived quantum defects have values appropriate for Rydberg orbitals centred on the fluorine atoms. This is to be expected since these three outer-valence molecular orbitals of GeF_4 are essentially F $2p\pi$ non-bonding orbitals and do not involve the central Ge atom [26]. Also as expected, the lowest principal quantum number for Rydberg transitions originating from these fluorine-centred orbitals is $n = 3$. Our assignments are in excellent agreement with those of the EELS study of Kuroki et al. [7], but like them we find that multiple assignments are possible for some of the Rydberg transitions, especially those at higher excitation energies. It should be noted that there is little resemblance in the intensity distribution of our fluorescence excitation spectrum (Fig. 1a) and the electron energy loss spectrum over this 13–17 eV range. This is not unexpected, since our experiment only detects those Rydberg states of GeF_4 which dissociate to a fluorescing excited state of a fragment, whereas EELS observes all the Rydberg states whose transitions from the ground state are allowed by optical selection rules. Furthermore, both spin and orbital selection rules are not particularly strict with EELS, especially at high scattering angles, so that more peaks are observed than in the fluorescence excitation spectrum over the same region.

We consider now the products of the photodissociation of these Rydberg states of GeF_4. By comparison with previous higher-resolution studies of the $\tilde{A}\,^1B_1$–$\tilde{X}\,^1A_1$ and $\tilde{a}\,^3B_1$–$\tilde{X}\,^1A_1$ transitions in GeF_2 [16–18], the bands spanning the wavelength 215–265 and 300–380 nm ranges in Fig. 2 are assigned to GeF_2 $\tilde{A}$–$\tilde{X}$ and $\tilde{a}$–$\tilde{X}$, respectively. Both these transitions in SiF_2 were observed in our recent VUV photoexcitation study on SiF_4 [2]. The experimental thresholds for production of the GeF_2 $\tilde{A}\,^1B_1$ and $\tilde{a}\,^3B_1$ states, 14.0 ± 0.2 and 12.8 ± 0.2 eV, both lie between the calculated thresholds to form GeF_2^* with F_2 or 2F (Table 1). That is, the thermochemical threshold to form GeF_2^* with 2F lies over 1 eV above the experimental threshold of formation of GeF_2^*. There is therefore clear thermochemical evidence that both GeF_2 $\tilde{A}\,^1B_1$ and $\tilde{a}\,^3B_1$ must form from GeF_4^* in a one-step process with F_2 as the other product. It is assumed that the photodissociation pathway passes through a tightly constrained transition state, with two Ge–F bonds breaking simultaneous with one F–F bond forming. This behaviour of $GeF_4^* \rightarrow GeF_2^*$ should be contrasted with the analogous photodissociation in SiF_4^* [2], where SiF_2 $\tilde{A}\,^1B_1$ and $\tilde{a}\,^3B_1$ both have experimental thresholds very close to the thermochemical energy to form SiF_2^* with two fluorine atoms. Although in this instance there was no direct thermochemical evidence, nevertheless it was assumed that both photodissociations probably occur as a two-step, sequential process via an excited state of SiF_3, i.e. $SiF_4^* \rightarrow SiF_3^* + F \rightarrow SiF_2^* + F + F$. Assuming that the thermochemical data given by Harland et al. [14] is correct, and that GeF_2^* can therefore only form in conjunction with F_2, it should also be noted that photodissociation of GeF_4^* singlet Rydberg states via a single-step process to GeF_2 $\tilde{a}\,^3B_1 + F_2$ $X\,^1\Sigma_g^+$ (the major product channel) is a spin-forbidden process. There are no triplet states of F_2 of low enough energy to form in conjunction with GeF_2 $\tilde{a}\,^3B_1$. This photodissociation process can therefore only be spin-allowed either if the initially populated Rydberg states of GeF_4 have predominantly triplet spin character or if rapid inter-system crossing to a triplet state occurs. We should also note that photodissociation of low-lying Rydberg states of $GeCl_4$ predominantly produces $GeCl_2$ $\tilde{a}\,^3B_1$, with the spin-allowed route to $GeCl_2$ $\tilde{A}\,^1B_1$ being a very minor channel [8]. In this instance, it was not possible to determine from thermochemistry whether the other product was Cl_2 or 2Cl. Dissociation of singlet Rydberg states of GeX_4 to GeX_2 $\tilde{A}\,^1B_1 + X_2$ $X\,^1\Sigma_g^+$ is, of course, spin-allowed.

The lifetimes of the $\tilde{A}\,^1B_1$ and $\tilde{a}\,^3B_1$ states of GeF_2 have not been measured before. Their values reported here show no surprises. The $\tilde{A}\,^1B_1$–$\tilde{X}\,^1A_1$ fluorescence band of GeF_2 is both orbitally and spin allowed, and the value measured of 9.3 ± 0.1 ns is entirely appropriate for such an electronic transition in the UV. The $\tilde{A}\,^1B_1$ state of SiF_2 shows a similar value, 9–12 ns in this study and 11.2 ± 1.5 ns in our earlier study [2]. The lifetime of the $\tilde{a}\,^3B_1$ state of GeF_2 is too long to measure using our experimental technique, and we can only place a lower limit, ca. 500 ns, on the lifetime of this state; its value could easily be one or two orders of magnitude greater. This is as expected for the spin-forbidden $\tilde{a}\,^3B_1$–$\tilde{X}\,^1A_1$ phosphorescence process. The lifetime of the

analogous $\tilde{a}\,^3B_1$ state of $GeCl_2$ was also too long to measure in our experiment [8], but has been measured independently to be 17.4 ± 0.6 μs [27]. Perhaps the most interesting aspect of the GeF_2 $\tilde{a}\,^3B_1$ lifetime measurement, however, is the absence of the fast decay component which is observed from the analogous state of SiF_2, 2.6 ± 0.4 ns in our earlier study [2] and 3.3 ± 0.4 ns in this study (Fig. 3d). It seems very unlikely that this value for SiF_2 $\tilde{a}\,^3B_1$ is a lifetime for radiative decay, but more likely represents a lifetime for fast non-radiative inter-system crossing to high vibrational levels of the ground state of SiF_2 [2,28,29]. This decay channel is clearly not present in GeF_2. This might be considered surprising, given the predicted larger spin–orbit coupling matrix element linking the $\tilde{a}\,^3B_1$ and $\tilde{X}\,^1A_1$ states due to the larger atomic spin–orbit coupling constant of the Ge atom.

We now discuss two fluorescence channels that are not observed. The simplest photodissociation channel for low-lying Rydberg states of GeF_4 is cleavage of one Ge–F bond to form the GeF_3 free radical. Unlike CF_4 and SiF_4 where photodissociation of the lowest Rydberg states does indeed lead to fluorescence in the CF_3 and SiF_3 radicals [1,2], fluorescence from excited states of GeF_3 has not been observed in our experiment. This could be due to a number of reasons. First, photodissociation by a single Ge–F bond cleavage is a very minor channel. Second, photodissociation only produces the ground state of GeF_3. Third, there are no excited states of GeF_3 that fluoresce in the range of the UV/visible that our experiments can detect (190–500 nm). At the other extreme, cleavage of all the bonds in GeF_4 can leave Ge atoms in excited fluorescing states. This process was observed with $GeCl_4$ [8], and UV emission was observed in the Ge atom with the strongest emission at 267 nm. This emission is the $^3P_1(4p^15s^1)$–$^3P_0(4p^2)$ transition, and it was found that the experimental threshold for production of $Ge^*(^3P_1)$ corresponded to the thermochemical energy of $Ge^* + 4Cl$ (18.8 eV) [8]. Emission in the Ge atom is not observed in this GeF_4 study. The simplest explanation is that the stronger Ge–F bond causes the energy of the $Ge^* + 4F$ channel to lie at the higher energy of 26.1 eV (Table 1), outside the range of the primary monochromator used in these experiments.

Emission from the $\tilde{D}\,^2A_1$ state of GeF_4^+ (adiabatic IE = 21.1 eV) has been observed before using a variety of excitation sources [9,20,21], and the results presented here, whilst confirming data obtained elsewhere, yield no new information on the spectroscopic properties of this state. In our earlier time-resolved study at Daresbury using single-bunch pulsed photoexcitation, bi-exponential decay from this state was observed with τ_1 and τ_2 values of 3.1 and 6.3 ns [9]. We see no evidence for double exponential behaviour in the analyses of the time-resolved spectra obtained in this study, and we obtain a very accurate single value for the lifetime of this state, 5.02 ± 0.01 ns. Given the superior method of analysing the single-bunch lifetime decays, in particular the manner in which the effects of the instrument function are now deconvoluted from the experimental data [11], we believe this value of 5.02 ns is the superior value for the lifetime of the $\tilde{D}\,^2A_1$ state of GeF_4^+. Although not stated at the time of our earlier study [9], it is difficult to explain how the decay of the fluorescence from this state could be anything other than a single-exponential function.

Acknowledgements

We thank Dr. K.M. Weitzel for the loan of a multi-channel analyser and PC for these experiments. KJB and DPS thank EPSRC for Research Studentships, KJB thanks the Daresbury Laboratory for a CASE award. The EU Human Capitol and Mobility programme (Contract Number ERBFMGE-CT-950031) and the British Council (ARC bilateral programme with Germany, Contract Number 707) are thanked for funding of this work. Finally, we thank Dr. H. Biehl for help with recording the spectra.

References

[1] H. Biehl, K.J. Boyle, R.P. Tuckett, H. Baumgärtel, H.W. Jochims, Chem. Phys. 214 (1997) 367.
[2] H. Biehl, K.J. Boyle, D.P. Seccombe, D.M. Smith, R.P. Tuckett, K.R. Yoxall, H. Baumgärtel, H.W. Jochims, J. Chem. Phys. 107 (1997) 720.
[3] V.M. Donnelly, D.L. Flamm, J. Appl. Phys. 51 (1980) 5273.
[4] L.C. Lee, X. Wang, M. Suto, J. Chem. Phys. 85 (1986) 6294.
[5] M. Suto, X. Wang, L.C. Lee, T.J. Chuang, J. Chem. Phys. 86 (1987) 1152.

[6] T. Ibuki, N. Washida, U. Itoh, Y. Toyoshima, H. Onuki, Chem. Phys. Lett. 136 (1987) 447.
[7] K. Kuroki, D. Spence, M.A. Dillon, J. Elect. Spectrosc. Rel. Phenom. 70 (1994) 151.
[8] H. Biehl, K.J. Boyle, D.P. Seccombe, D.M. Smith, R.P. Tuckett, H. Baumgärtel, H.W. Jochims, J. Elect. Spectrosc. Rel. Phenom. (1998) in press.
[9] I.R. Lambert, S.M. Mason, R.P. Tuckett, A. Hopkirk, J. Chem. Phys. 89 (1988) 2683.
[10] K.J. Boyle, Ph.D. Thesis, University of Birmingham, 1998.
[11] C.M. Gregory, M.A. Hayes, G.R. Jones, E. Pantos, Technical Memorandum, Daresbury Laboratory, reference DL/SCI/TM98E, 1994.
[12] P.J. Bassett, D.R. Lloyd, J. Chem. Soc. A. (1971) 641.
[13] S. Cradock, Chem. Phys. Lett. 10 (1971) 291.
[14] P.W. Harland, S. Cradock, J.C.J. Thynne, Int. J. Mass Spectrosc. Ion Process. 10 (1972) 169.
[15] J. Emsley, The Elements, 2nd edn., OUP, 1996.
[16] R.W. Martin, A.J. Merer, Can. J. Phys. 51 (1973) 727.
[17] S. Yagi, N. Takahashi, Appl. Phys. Lett. 61 (1992) 2677.
[18] R. Hauge, V.M. Khanna, J.L. Margrave, J. Mol. Spectrosc. 27 (1968) 143.
[19] N. Washida, M. Suto, S. Nagase, U. Nagashima, K. Morokuma, J. Chem. Phys. 78 (1983) 1025.
[20] S.M. Mason, R.P. Tuckett, Mol. Phys. 62 (1987) 979.
[21] H. Van Lonkhuyzen, J.F.M. Aarts, Chem. Phys. Lett. 140 (1987) 434.
[22] J.F.M. Aarts, S.M. Mason, R.P. Tuckett, Mol. Phys. 60 (1987) 761.
[23] S.M. Mason, R.P. Tuckett, Mol. Phys. 60 (1987) 771.
[24] M. Suto, J.C. Han, L.C. Lee, T.J. Chuang, J. Chem. Phys. 90 (1989) 2834.
[25] C.E. Theodosiou, M. Inokuti, S.T. Manson, At. Data Nucl. Data Tables 35 (1986) 473.
[26] R.N. Dixon, R.P. Tuckett, Chem. Phys. Lett. 140 (1987) 553.
[27] T. Ibuki, Chem. Phys. Lett. 169 (1990) 64.
[28] J. Karolczak, R.H. Judge, D.J. Clouthier, J. Am. Chem. Soc. 117 (1995) 9523.
[29] D.J. Clouthier, private communication.